LUPINE PUBLISHERS

Modern Approaches on Material Science

DOI: 10.32474/MAMS.2020.02.000146

ISSN: 2641-6921

Research Article

Probing into Dopant Concentration Dependent Luminescence Properties of Transition Metal Mn^{2+} Activated Ca- α-SiAlON Orange-Red Phosphors

Ni J[1,2], Zhou ZZ[1], Xu XK[1], Liu Q[1,2]*, Shen FR[3,4], and He LH[3,5,6]**

[1]*The State Key Laboratory of High-Performance Ceramics and Superfine Microstructures, Shanghai Institute of Ceramics, Chinese Academy of Sciences, China*

[2]*Center of Materials Science and Optoelectronics Engineering, Beijing ,China*

[3]*Institute of Physics, Chinese Academy of Sciences, Beijing , China*

[4]*School of Physical Sciences, Beijing ,China*

[5]*Songshan Lake Materials Laboratory, Dongguan, China*

[6]*Spallation Neutron Source Science Center, Dongguan, China*

****Corresponding author:** *Liu Q, Shanghai Institute of Ceramics, Chinese Academy of Sciences, Shanghai, China

** He LH, Institute of Physics, Chinese Academy of Sciences, Beijing, China

Received: February 29, 2020 **Published:** March 11, 2020

Abstract

Transition metal (TM) Mn^{2+} activated Ca-α-SiAlON phosphors with compositions of $Ca1-_xSi_9Al_3ON_{15}:xMn^{2+}$ (x=0.02~0.16) have been designed and synthesized through a high temperature solid-state reaction. In the polyhedron structure of Ca-α-SiAlON host (P31c), Mn^{2+} ions can be accommodated in the lattice without destabalizing the crystal structure, which has been revealed by both XRD and neutron powder diffraction (NPD) characterization. The successful doping of TM Mn^{2+} in host was further confirmed by magnetic susceptibility characterization and the occupation of Mn^{2+} in lattice was analyzed through Rietveld refinement of crystal structure. The slight left-shift of diffraction peaks in XRD patterns and Gaussian fitting sub-bands of emission spectra all proved that the activators Mn^{2+} in Ca-α-SiAlON host not only incorporate into the "separated interstitial sites", but also modestly substitute for Al^{3+} sites. The phosphors mainly deliver orange-red emission centered at ~600nm under UV excitation, which is ascribed to the typical characteristic $^4T_1(^4G)\rightarrow{}^6A_1(^6S)$ electron transition of divalent Mn^{2+}. The highest photoluminescence (PL) intensity arrives at x=0.12 of Mn^{2+} doping concentration in compositions, then the doping concentration quenching occurs. In addition, through calculating the critical transfer distance, it indicates that the dipole-quadrupole (d-q) interaction is the major mechanism for doping concentration quenching in the phosphors. With the increment of Mn^{2+} content up to x=0.12 (quenching concentration), the decay time τ decreases monotonically from 7.5 to 5.5μs, ascribed to the non-radiative energy migration among Mn^{2+} ions in the phosphors.

Keywords: Ca-α-SiAlON: Mn^{2+} phosphor; Magnetic susceptibility; Neutron diffraction; Gaussian fitting; Dipole-quadrupole interaction

Abbreviations: LED: light emitting diodes; CCT: Correlated Color Temperature; TM: transition metal; CRI: Color Rendering Index; NPD :Neutron powder diffraction; TOF: time-of-flight; GPPD: general purpose powder diffractometer; CSNS: China Spallation Neutron Source; GSAS: General Structure Analysis System; MPMS: Magnetic Property Measurement System

Introduction

With the increasing awareness of environmental protection and energy saving, LEDs (light emitting diodes) have gradually became the major source for solid-state lighting. Currently, the commercial white-LED (w-LED) devices sold on the market are using yellow-emitting phosphor ($Y_3Al_5O_{12}:Ce^{3+}$ or simply YAG: Ce) with a blue chip (InGaN). The disadvantages of this device, especially for the lamp purpose, are lower Color Rendering Index (CRI, R_a < 75)

and higher Correlated Color Temperature (CCT) due to lacking red light [1,2]. To make up for this drawback, researchers have tried to add red phosphors for supplementary, even using red and green phosphor mixture together with a blue chip directly [3,4], or using UV (ultraviolet) chip to excite blue, green, and red phosphor mixture [5]. Hereby, the stable red phosphors with good luminescent properties are highly required in any preparation methods. At present, the red phosphors normally utilize either trivalent rare earth ions such as $Eu^{3+,}$ $Pr^{3+,}$ $Sm^{3+,}$ Tb^{3+} as the luminous centers in sulfides [6], tungstates [7], titanates [8], powellite [9], etc., or divalent Eu^{2+} in nitride $M_2Si_5N_8$ [10] and $CaAlSiN_3$ [11]. The chemical stability of the former phosphors is not very good, and the preparation methods of the latter phosphors are a litter difficult. On account of rich oxidation state variation and great optical properties, the transition metal (TM) Mn ions doped oxide, fluoride, sulfide, and nitride phosphors have been extensively investigated [12-31]. Mn ions as activators in varied phosphors may possess different valence states, while the most common is the divalent manganese ($Mn^{2+)}$ or quadrivalent manganese (Mn^{4+}).

Due to the vibrational modes of $^2E_g \rightarrow {}^4A_{2g}$ transition for the $3d_3$ electrons, Mn^{4+} always shows a linear red emission in some oxides [12-15] and fluorides [16-21] with a high correlated color temperature (CCT) and low color rendering index (CRI). As for the $Mn^{2+,}$ it usually shows a broad band emission from green to deep red emission owing to the electron transition of $^4T_1(^4G) \rightarrow {}^6A_1(^6S)$ of $Mn^{2+,}$ in which the lowest excitation level $^4T_1(^4G)$ decreases with the increase of the crystal field of host, resulting in the red-shift of emission [22,23]. Therefore, the color of emission is strongly dependent on the crystal field strength of the host lattice and the coordination number of Mn^{2+} with neighboring atoms. Generally, Mn^{2+} usually delivers a green emission in weak crystal-field site or with low tetrahedral coordination number [24,25], whereas it shows an orange to deep red emission on a strong crystal-field site or higher octahedral coordination number [26-31]. Namely, the crystal-field and coordination number exhibit a great effect on the emission color of phosphors. Otherwise, the stronger nephlauxetic effect from nitrides and oxynitrides can also enhance the crystal field splitting, which increases the stokes-shift and spectral-shift. Furthermore, the polyhedral oxynitride Ca-α-SiAlON (P31c) is a host material with strong nephlauxetic effect and high coordination number. It possesses an extraordinary chemical and thermal stability, for it consists of stiff three-dimensional tetrahedral [(Si, Al) $(N, O)_4$] networks [32,33]. Accordingly, it is proposed that the smaller Mn^{2+} ion as a promising and abundant non-rare-earth dopant would lead to red emission under excitation when introduced in Ca-α-SiAlON. In the present work, single Mn^{2+} activated Ca-α-SiAlON phosphors were designed and successfully prepared. The dopant's existence and location, dopant's concentration effect on emission, and energy transfer mechanism of Mn^{2+} in Ca-α-SiAlON host have been systematically explored, using advanced magnetic susceptibility measurement, neutron diffraction characterization, et al.

Experimental Work

Synthesis of Ca- α-SiAlON: Mn^{2+} Phosphors

Mn^{2+} single doped Ca-α-SiAlON powders were prepared by a solid-state reaction method. The specific composition is expressed as $Ca_{1-x}Si_9Al_3ON_{15}$:xMn^{2+} and Mn^{2+} doping concentrations range from 0.02 to 0.16 (x=0.02, 0.04, 0.06, 0.08, 0.10, 0.12, 0.14, 0.16). The starting materials used in preparation of these samples were α-Si_3N_4 (SN-E10, Ube Industries, Japan), AlN (Grade A, Starck Industries, German), $CaCO_3$ (Sinopharm Chemical Reagent Co., Ltd, china) and $MnCO_3$ (Sinopharm Chemical Reagent Co., Ltd, china). The pre-weighed powders were mixed up by ball-milled method in ethanol for 12h. Then the mixture powders were dried at 80 °C for 6h. After entirely ground, the appropriate mixture powders were transferred into BN crucibles and calcined at 1600 °C for 4h under N_2 atmosphere in a graphite furnace at a heating rate of 5 °C/min. The calcination temperature of 1600 °C/4h is an optimal parameter based on our previous work. Finally, the cooled powders were ground twice for further measurements and characterizations.

Characterization and Measurements

The crystal phase of as-prepared samples were identified by X-ray diffractometer (D8 ADVANCE, Bruker, Germany) with CuK_α radiation (λ=0.1541 nm), in a 2θ range of 20° to 80°. Neutron powder diffraction (NPD) was performed at time-of-flight (TOF) general purpose powder diffractometer (GPPD) at China Spallation Neutron Source (CSNS). Neutron diffraction patterns were collected at room temperature with wavelength band from 0.1 to 4.9Å. The crystal structure and occupation of Mn ions in the host were refined by the Rietveld method using the General Structure Analysis System (GSAS) suite of programs. The magnetic susceptibility was tested by Magnetic Property Measurement System (MPMS, SQUID, Quantum Design, USA) to confirm the successful doping of magnetic TM Mn^{2+} ions in host. The photoluminescence measurements (excitation and emission spectra, PLE and PL) of phosphors $Ca_{1-x}Si_9Al_3ON_{15:\ x}Mn^{2+}$ with varied Mn^{2+} concentration (x=0.02-0.16) were performed at room temperature to determine the doping concentration dependent photoluminescence properties, on a F-4600 spectrometer (Hitachi, Japan) with a 150 W xenon lamp as excitation. The decay curves of Mn^{2+} lifetime values were recorded on a lifetime and steady state spectrometer (FLS 980, Edinburgh Instruments, UK), with a lifetime measurement range of 1 μs ~10 s (μF2).

Results and Discussion

Crystal Structure of Ca- α -SiAlON: Mn^{2+} Phosphors

It has been found that all the prepared phosphors $Ca_{1-x}Si_9Al_3ON_{15}$:xMn^{2+} are isostructural and crystallized in its hexagonal host Ca-α-SiAlON (P31c), as shown in Figure 1, with a standard reference XRD pattern of Ca-α-SiAlON at the bottom of the figure (JCPDS card No. 33-0261). However, among the different Mn^{2+}

concentration, the prepared compounds show a high-purity phase with a lower Mn^{2+} doping concentration x=0.02 and 0.04. The trace of impurity phase is found when the doping concentration increases above 0.04. The impurity phase is identified as AlN and marked with "◆" in (Figure1) (AlN: JCPDS card No.25-1133), which is derived from the residual incompletely reacted AlN raw material. This phenomenon reveals a quite low solid solubility of Mn^{2+} ions in Ca-α-SiAlON host and the solubility plays an important role in the solid-state reaction to synthesize highly pure Ca-α-SiAlON: Mn^{2+} phase at 1600 °C. Theoretically, there exist two specially "separated interstitial sites" per unit cell in the α-SiAlON crystalline structure, one is a rectangle site with 0.10 x 0.24 nm in two-dimensional scale and another is a circular site with a 0.15nm diameter [34]. Relative to the Mn^{2+} ion radius (0.067nm in ionic radius), the interstitial site is large enough to be occupied by Mn^{2+} ion.

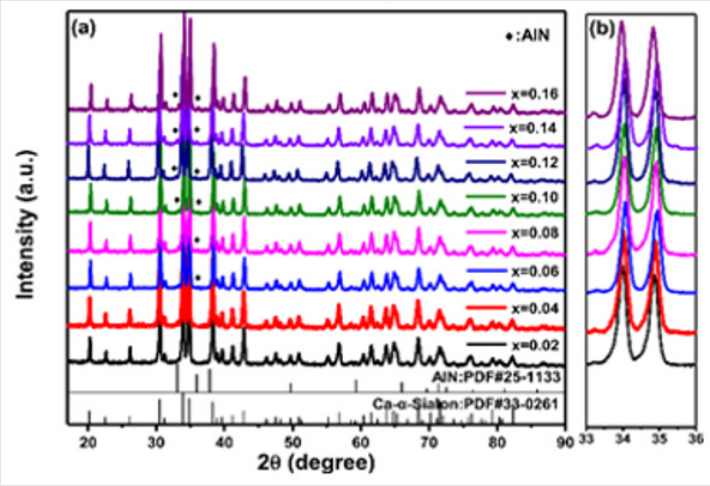

Figure 1: (a) XRD patterns of Ca-α-sialon: xMn^{2+} (x=0.02-0.16) phosphors synthesized at 1600°C, (b) the magnified regions of XRD patterns in a 2θ range of 33° ~ 36°.

Presuming that all the introduced small Mn^{2+} ions prefer to substitute Ca^{2+} sites (normally occupied at the interstitial sites) or incorporate into the unoccupied separated interstitial sites in Ca-α-SiAlON host, in this case, the XRD diffraction spectra would not be changed and lattice parameters could not be influenced. However, under accurate examination, it has been found that the XRD diffraction peaks in the selected 2θ region from 33° to 36° gradually shift to lower 2θ angles with increasing of Mn^{2+} concentration up to x=0.16 (seen in Figure1b), implying a slight lattice expanding caused by a portion of Mn^{2+} ions substituting for smaller Al^{3+} (0.0535nm in ionic radius) or perhaps Si^{4+} (0.0400nm in ionic radius). From another angle, in Ca-α-SiAlON host, the bond length of Al-N, Al-O, Si-N and Si-O was estimated to be ~1.87 Å, ~1.75 Å, ~1.74 Å, and ~1.62 Å, respectively [35-37], while, the bond length of Mn-N and Mn-O was statistic to be ~1.86Å and ~1.79Å in some nitrides and oxides [38-41]. Therefore, Mn^{2+} ions have more possibilities to replace Al^{3+} sites (MnAl) rather than Si^{4+} sites. This result further demonstrates that the introduction of more Mn^{2+} ions could result in a difficult solid-solution and then hamper the reaction of AlN with other starting powders, which produced the AlN impurities ultimately. Besides, in order to further confirm the incorporation and location of Mn^{2+} in its host, neutron powder diffraction (NPD) studies were performed for the compound Ca-α-SiAlON:$0.12Mn^{2+}$. Among all the prepared compounds, we selected the compound of Ca-α-SiAlON:$0.12Mn^{2+}$, because it shows the highest emission intensity under UV excitation. The NPD patterns were collected at room temperature by time-of-flight (TOF) general purpose powder diffractometer (GPPD).

In (Figure 2), it shows the NPD pattern of Ca-α-SiAlON:$0.12Mn^{2+}$, together with Bragg position, the calculated pattern, and the difference between experimental and calculated patterns. The atomic positions and occupations in the compound Ca-α-SiAlON:$0.12Mn^{2+}$ from detailed refinement results of the NPD pattern are listed in Table 1, from which it can been seen that the doped emitting centers of Mn^{2+} are almost occupied at Ca^{2+} sites In addition, to confirm the successful dilute doping of Mn_{2+} in Ca-α-SiAlON matrix, the magnetic susceptibility measurement, which is sensitive to magnetic TM Mn^{2+} addition, was carried out and the results of Moment-Magnetic Field (M-H) curves are indicated in (Figure 3), for three comparative compounds: un-doped Ca-α-SiAlON, low-doping Ca-α-SiAlON:$0.02Mn^{2+}$, and heavy-doping Ca-α-SiAlON:$0.12Mn^{2+}$. Normally, the Ca-α-SiAlON host as a semiconductor is a type of anti-magnetic material, however, it gradually turns into a ferromagnetic material as the Mn^{2+} doping concentration increases, as shown in Figure 3. According to the magnetic susceptibility results measured at 2K and 300K for the three comparative compounds, the magnetic susceptibility change also proves that Mn^{2+} ions have been incorporated into the lattice of host.

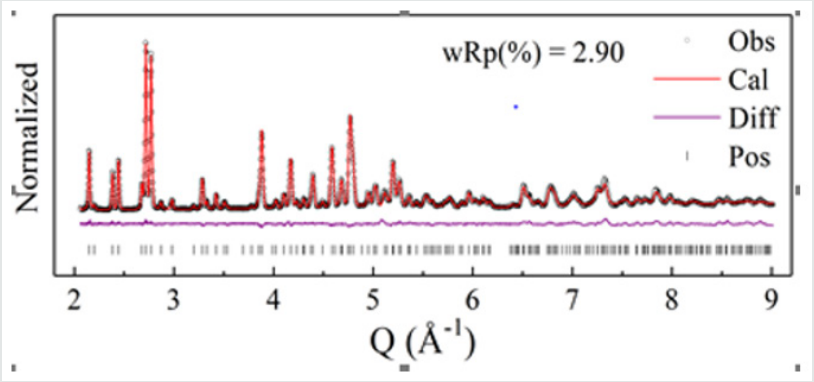

Figure 2: Neutron powder diffraction pattern of Ca-α-sialon:0.12Mn^{2+}, together with Bragg position (black circle), the calculated pattern (red line), and the difference (purple line) between experimental and calculated patterns, and peak position (black bar), collected at room temperature by GPPD.

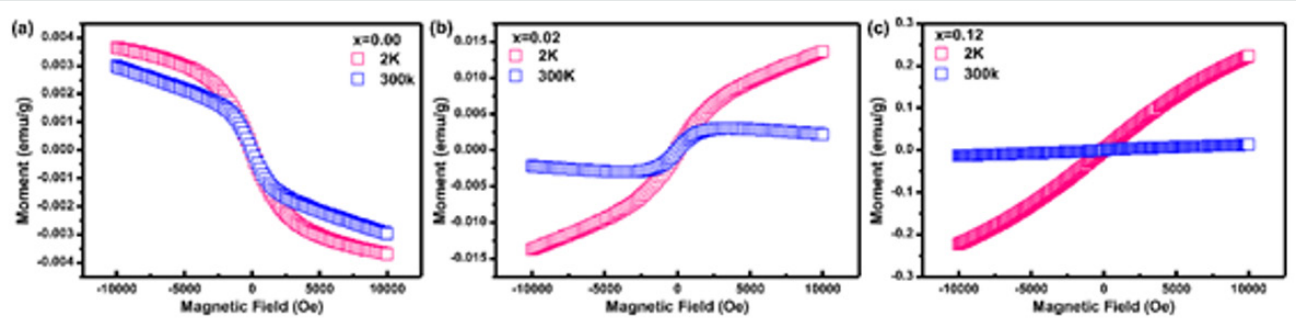

Figure 3: Magnetic susceptibility of M-H curves on, (a) un-doped Ca-α-sialon host; (b) Ca-α-sialon:0.02Mn^{2+} phosphor, and (c) Ca-α-sialon:0.12Mn^{2+} phosphor.

Table 1: Atomic positions and occupations of Ca-α-sialon: 0.12Mn^{2+}, with lattice constants a=b=7.8565(2)Å, c=5.7166(1)Å.

Atoms	X	Y	Z	Occupation
Ca	0.3333	0.6667	0.249(4)	0.72(2)
Mn	0.3333	0.6667	0.249(4)	0.28(2)
Si_1	0.511(1)	0.079(1)	0.210(1)	0.69(4)
Al_1	0.511(1)	0.079(1)	0.210(1)	0.31(4)
Si_2	0.1683(6)	0.2523(5)	-0.008(2)	0.69(4)
Al_2	0.1683(6)	0.2523(5)	-0.008(2)	0.31(4)
N_1	0	0	-0.008(2)	0.932(6)
O_1	0	0	-0.008(2)	0.068(6)
N_2	0.3333	0.6667	0.642	0.932(6)
O_2	0.3333	0.6667	0.642	0.068(6)
N_3	0.3400(4)	-0.0509(3)	-0.017(1)	0.932(6)
O_3	0.3400(4)	-0.0509(3)	-0.017(1)	0.068(6)
N_4	0.3169(3)	0.3151(4)	0.240(1)	0.932(6)
O_4	0.3169(3)	0.3151(4)	0.240(1)	0.068(6)

Luminescence Properties of Ca-α-SiAlON: Mn^{2+} Phosphor

The representative photoluminescence excitation and emission spectra of Ca-α-SiAlON:0.02Mn^{2+} and Ca-α-SiAlON:0.12Mn^{2+} phosphors are illustrated in (Figure 4) 4a & 4b. The excitation spectra monitored at 600nm comprise one dominant band centered at 265nm and other weak bands between 350nm to 450nm. The 265nm band is related to the band gap absorption [42] and the weak bands are ascribed to the transitions of Mn^{2+} from the ground state $^6A_1(^6S)$ to excited states $^4T_2(^4D)$, $[^4A_1(^4G), ^4E(^4G)]$ and $^4T_1(^4G)$ levels, respectively [25,43-45]. Because d-d electron transition of Mn^{2+} is parity spin-forbidden, these excitation bands between 350nm to 450nm are very weak. For all the prepared

compounds, two wider and stronger emission peaks are observed in PL spectra under UV light excitation of 265nm. One stronger dominant orange-red emission with a maximum at ~600nm is from the typical emission of Mn^{2+}, corresponding to the energy transition $^4T_1(^4G) \rightarrow {}^6A_1(^6S)$ of Mn^{2+} in the highly coordinated nitride and oxide host lattice [25,45-48]. Another emission band ranging from 350nm to 550nm shows a wider UV-green emission possibly assigned to the oxygen-related defects (mainly oxygen vacancy) in the host lattice. The presumed oxygen defects have elucidated and proved by the Electron Paramagnetic Resonance (general purpose powder diffractometer) spectra examination in another separated work [42]. The oxygen-related defects are possibly developed in the high temperature synthesis process of phosphors in a reductive N_2 environment. Otherwise, the strong orange-red emission band peaked at ~600nm is apparently asymmetry and could be divided into several emissions.

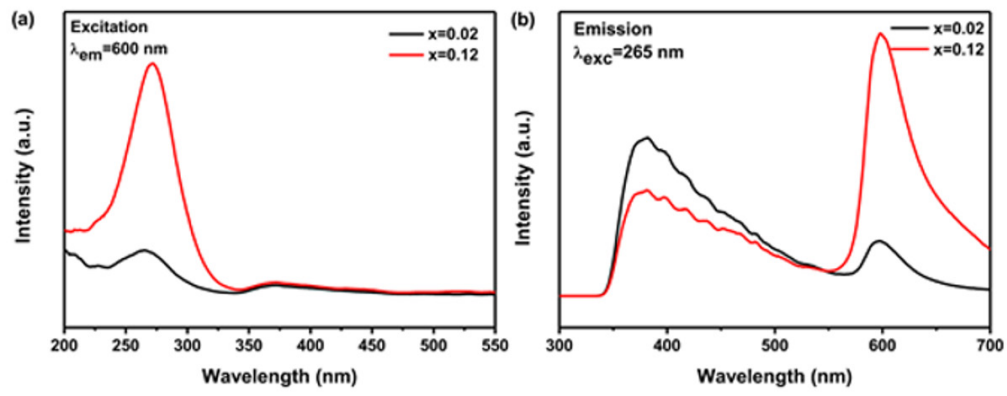

Figure 4: Excitation (λ_{em}=600nm); and emission (λ_{exc}=265nm); spectra of Ca-α-sialon:0.02Mn^{2+} and Ca-α-sialon:0.12Mn^{2+} phosphor samples.

If only the interstitial sites in Ca-α-SiAlON host are substituted by Mn^{2+} ions, perhaps it is expected to just show three narrow symmetrical emission bands in the luminescence spectra (depicted in Figure5a), since Mn^{2+} ions occupied at lattice interstitial sites were proposed to be coordinated by seven (O,N) anions in three different M-(O, N) distances, named as Mn(1), Mn(2), and Mn(3), based on the crystal structure refinement analysis [49]. While, contrasting to Figure 5b, the orange-red emission should be better separated into four sub-bands by Gaussian fitting, which are centered averagely at 589nm, 600nm, 618nm and 650nm, respectively, demonstrating four different emission sites in the representative Ca-α-SiAlON:0.12Mn^{2+} phosphor. According to the above-mentioned, the emission bands from lower energy (600 nm or 16666cm^{-1}, 618nm or 16181cm^{-1}, and 650nm or 15384cm^{-1}) should originate from the Mn^{2+} locating at interstitial sites, they are Mn(1), Mn(2), and Mn(3) with seven (O,N) anions coordination [49] (Figure 5). Another emission band from higher energy (589nm or 16978cm-1) might be assigned to the Mn^{2+} locating at Al^{3+} sites (MnAl) with four-fold (N.O) coordination [35-37]. The Gaussian fitting results of the asymmetry emission band in the Ca-α-SiAlON:0.12Mn^{2+} compound is quite similar to that in $CaAlSiN_3$:Mn^{2+} nitride phosphors [28]. In $CaAlSiN_3$:Mn^{2+}, there is only one crystallographic site for Ca^{2+} coordinated with five N and one site for Al^{3+} coordinated with four N. Thus, when heavily-doping, Mn^{2+} ions can occupy not only at pentahedrally coordinated Ca site (MnCa), but also at tetrahedrally coordinated Al site (MnAl) to some extent, then the asymmetry emission band is deconvoluted into two Gaussian sub bands centered at about 548nm and 627nm, respectively.

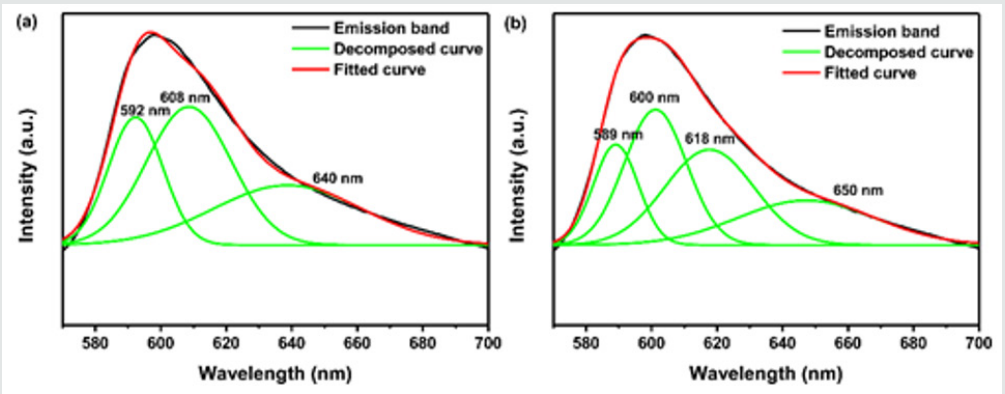

Figure 5: Emission (λ_{ex}=265nm) spectra of Ca-α-sialon:0.12Mn^{2+} phosphor sample with Gaussian fitting components: (a) separated into three sub-bands, (b) separated into four sub-bands.

Concentration Quenching and Decay Behavior of Ca-α-SiAlON: Mn^{2+} Phosphors

The dependence of emission intensity (peaked at ~600 nm) on Mn^{2+} ion concentration is given in (Figure 6). The emission intensity is maximized at the Mn^{2+} concentration around 12mol% and it is nearly five times of that for Ca-α-SiAlON:0.02Mn^{2+}, then the emission intensity diminishes with further increase of Mn^{2+} content, indicating a clear concentration quenching of emission above 12mol% of Mn^{2+} content. The concentration quenching phenomenon may be caused by the re-absorption of Mn^{2+} ions at a higher doping level and non-radiative energy transfer between Mn^{2+} and Ca-α-SiAlON host. Hence, the doping concentration dependent emission is very important for evaluating phosphors' properties. To deeply investigate the concentration quenching phenomena of our Ca-α-SiAlON:xMn^{2+} phosphors, the critical transfer distance (R_c) related to the Mn^{2+} concentration quenching can be estimated from the equation as follows, on account of the mechanism of energy transfer in phosphors pointed by Blasse-formula [50, 51]:

$$R_c \approx 2(3V / 4\pi x_c N)^{1/3} \quad (1)$$

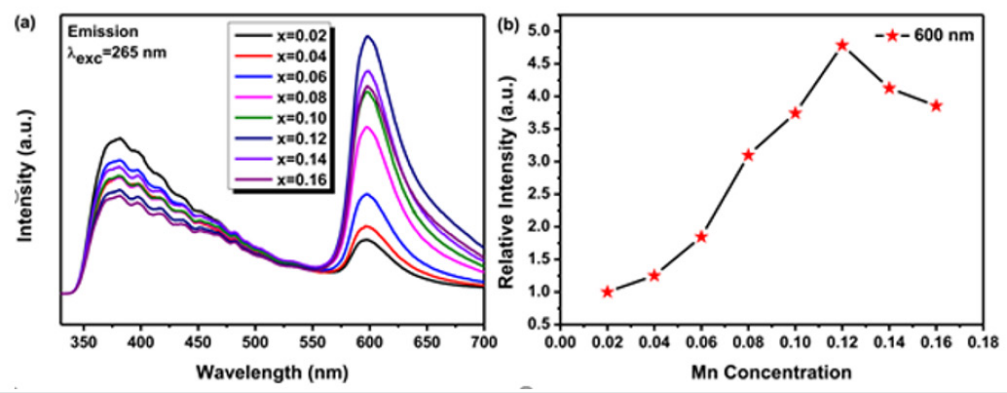

Figure 6: (a)Emission (λ_{excel}=26 nm) spectra of Ca-α-sialon:xMn^{2+} phosphors with various x from 0.02 to 0.16, (b) The curve of PL intensity of Ca-α-sialon: xMn^{2+} around ~600nm emission as a function of Mn^{2+}

Using this equation, V = 0.308nm^3 is the volume of the unit cell of Ca-α-SiAlON, N=2 is the number of dopant in the unit cell of Ca-α-SiAlON, and x_c = 0.12 is the critical quenching concentration of Mn^{2+}. The critical transfer distance (R_c) is calculated to be ~13.48Å, which is much longer than the typical critical distance (normally ~5Å for most phosphors [52]) responsible for forbidden transitions of Mn^{2+} via exchange interaction. Therefore, in Ca-α-SiAlON: xMn^{2+}, it hardly plays any role on the energy transfer among Mn^{2+} ions through exchange interaction. As a result, it is inferred that the concentration quenching does not take place via exchange interaction, while it is mainly governed by electric multipolar interaction, such as the situation in Eu^{2+} doped Ca-α-SiAlON [53-54]. Except the Blasse-formula, the critical distance R_c could be also obtained from Dexter's formula and given as follows [52,55]:

$$R_{6c}^{\ 6} = 3\times10^{12} \times f_d \int f_s(E) f_a(E) / E^4 dE \quad (2)$$

$$R_{8c}^{\ 8} = 3\times10^{12} \times \lambda_s^2 f_q \int f_s(E) f_a(E) / E^4 dE \quad (3)$$

Here, R_{6c} represents the dipole-dipole energy transfer distance, R_{8c} represents the dipole-quadrupole energy transfer distance, f_d = 10^{-7} and f_q = 10^{-10} are the oscillator strength for dipole-dipole and dipole-quadrupole electrical absorption transitions [56]. Then, the spectra overlap $\int f_s(E) f_a(E)/E^4 dE$ is estimated to be 0.0586eV^{-5}, which is extracted experimentally from the normalized excitation and emission spectra datum of our Ca-α-SiAlON:0.12Mn^{2+} compound, λ_s = 6000Å is the wavelength of maxima emission peak. Moreover, Eq. (2) indicates the dipole-dipole energy transfer mechanism between Mn^{2+} and Ca-α-SiAlON host, while Eq. (3) indicates the dipole-quadrupole energy transfer mechanism. According to the above formula (2), R_{6c} is calculated to be 5.1Å, which largely deviates from the result obtained from Blass-formula calculation result. Since the 3d electron transitions of Mn^{2+} is spin-forbidden, the possibility of a dipole-dipole interaction is very small in Mn^{2+} single doped host [57]. Whereas, R_{8c} is calculated to be 12.60Å, which is approximate to the previous datum of 13.48Å using Blass-formula calculation. Therefore, it is confirmed that the dipole-quadrupole (d-q) interaction is the major mechanism for concentration quenching in Ca-α-SiAlON: xMn^{2+} phosphors. To declare the luminescence lifetime of the produced Ca-α-SiAlON: xMn^{2+} phosphors, the room temperature lifetime curves of Mn^{2+} in Ca-α-SiAlON host (x=0.02 and 0.12) monitored at 600nm with 265nm excitation were measured and are displayed in (Figure 7). The decay curves could be approximately assessed using the empirical equation:

$$I(t) = A_1 \exp(-t/\tau_1) + A_2 \exp(-t/\tau_2) \quad (4)$$

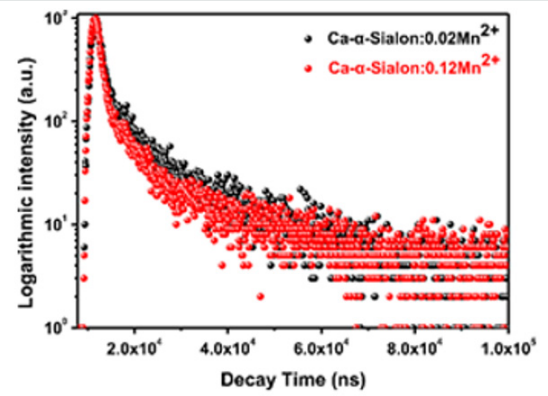

Figure 7: Decay curves of Ca-α-sialon:0.02Mn^{2+} and Ca-α-sialon:0.12Mn^{2+} phosphors under 265nm excitation and monitored at 600nm emission.

In this equation, I mean luminescence intensity; A_1 and A_2 are constants; t is testing time; τ_1 and τ_2 are the shorter and longer decay time calculated by Eq. (4). According to the above equation and our conducted computer fitting, τ_1 and τ_2 for the all prepared samples are listed in Table 2. The average lifetime constant (τ) can be estimated using the equation (5):

$$\tau = \left(A_1\tau_1^2 + A_2\tau_2^2\right) / \left(A_1\tau_1 + A_2\tau_2\right) \quad (5)$$

On the basis of Eq. (5), with the increment of Mn^{2+} content up to x=0.12 (concentration quenching), the decay time τ decreases monotonically from 7.5μs to 5.5μs shown in Table 2, ascribed to the non-radiative energy migration among Mn^{2+} ions. Otherwise, the decay curves fit well with the double-exponential decay mode, further confirming that it has more than one of luminescence center sites in Mn^{2+} doped Ca-a-SiAlON phosphors.

Table 2: The calculation results of short decay time, long decay time, and average decay time for Ca-α-sialon: xMn^{2+} (x=0.02-0.16) phosphors under 265nm excitation and monitored at 600nm emission.

x Value	τ_1 (ns)	A_1	τ_2 (ns)	A_2	τ_{av} (ns)
0.02	1310	1040	12690	129.6	7534.03
0.04	1269	1051	12480	107.4	6888.4
0.06	1178	969.2	12090	96.92	6680.55
0.08	1168	967.6	11790	96.06	6484.61
0.1	1121	1076	11560	87.6	5885.23
0.12	1094	1053	10470	98.23	5516.44
0.14	1148	1010	11480	96.24	6189.33
0.16	1168	1004	11910	93.06	6387.53

Conclusion

Transition metal Mn^{2+} single activated Ca-α-SiAlON orange-red phosphors have been successfully synthesized by solid-state reaction method. Research results on dopant concentration dependent luminescence properties of the phosphors can be summarized as follows: (1) All the prepared phosphors $Ca_{1-x}Si_9Al_3ON_{15}$:xMn^{2+} are isostructural and crystallized in its hexagonal host Ca-α-SiAlON (P31c), and emission centers Mn^{2+} have been incorporated into the lattice of host with Mn^{2+} mainly occupied at Ca^{2+} sites, conformed by using XRD analysis, neutron powder diffraction measurement, and magnetic susceptibility characterization. (2) The prepared phosphors exhibit a dominant asymmetry orange-red emission centered at ~600nm under 265nm (UV) excitation and the asymmetry emission band is deconvoluted into four Gaussian fitted sub-bands centered at 589nm, 600nm, 618nm and 650nm, respectively, indicating four different Mn^{2+} sites in Ca-α-SiAlON host. (3) It arrives the highest PL emission intensity at x=0.12 of Mn^{2+} doping concentration in $Ca_{1-x}Si_9Al_3ON_{15}$:xMn^{2+} compositions, that means the luminescence quenching concentration critical value x=0.12 in the series of $Ca_{1-x}Si_9Al_3ON_{15}$: xMn^{2+} compounds. (4) A litter far distance (R_{8c} = 12.60Å) energy transfer model via the dipole-quadrupole interaction has been deduced and considered to be the major mechanism for doping concentration quenching in Ca-α-SiAlON: xMn^{2+} phosphors. (5) With the increment of Mn^{2+} content up to x=0.12 (concentration quenching), the decay time τ decreases monotonically from 7.5μs to 5.5μs, ascribed to the non-radiative energy migration among Mn^{2+} ions in the phosphors.

Acknowledgement

Many thanks for financial supports from the National Key Research and Development Program of China (Grant No.

2017YFB0703203) and the Research Program of Shanghai Sciences and Technology Commission Foundation (Grant No. 18511110400).

References

1. Holonyak N, Bevacqua SF (1962) Coherent (visible) Light Emission from Ga ($As_{1-x}P_x$) Junctions. Appl Phys Lett 1(4): 82-83.
2. Lin, CC, Zheng YS, Chen HY, Ruan CH (2010) Improving Optical Properties of White LED Fabricated by a Blue LED Chip with Yellow/Red Phosphors. J Electrochem Soc 157(9): H900-H903.
3. Wu H, Zhang XM, Guo CF, Xu J (2005) Three-band white light from InGaN-based blue LED chip precoated with Green/red phosphors. IEEE Photonics Tech Lett 17(6): 1160-1162.
4. Hoppe HA (2009) Recent developments in the field of inorganic phosphors. Angew Chem Int Ed Engl 48(20): 3572-3582.
5. Sheu JK, Chang SJ, Kuo CH, Su YK (2003) White-light emission from near UV InGaN-GaN LED chip precoated with blue/green/red phosphors. IEEE Photonics Tech Lett 15(1): 18-20.
6. Jia D, Hunter DN (2006) Long persistent light emitting diode. J Appl Phys 100(11): 113-125.
7. Wen D, Feng J, Li J, Shi J (2015) K_2Ln (PO_4) (WO_4): Tb^{3+}, Eu^{3+} (Ln = Y, Gd and Lu) phosphors: highly efficient pure red and tuneable emission for white light-emitting diodes. J Mater Chem C 3(9): 2107-2114.
8. Zhang JC, Wang XS, Yao X (2010) Enhancement of luminescence and afterglow in $CaTiO_3$:Pr_3+ by Zr substitution for Ti. J Alloys Compd 498(2): 152-156.
9. Thomas M, Prabhakar Rao P, Deepa M, Chandran MR, et al. (2009) Novel powellite-based red-emitting phosphors: $CaLa_{1-x}NbMoO_8$:xEu^{3+} for white light emitting diodes. J Solid State Chem 182(1): 203-207.
10. Schlieper T, Milius W, Schnick W (1995) Nitrido-silicate II [1] Hochtemperatur-Synthesen und Kristallstrukturen von $Ba_2Si_5N_8$ und $Ba_2Si_5N_8$. Zeitschrift für anorganische und allgemeine Chemie 621(8): 1380-1384.
11. Piao X, Machida K, Horikawa T, Hanzawa H (2007) Preparation of $CaAlSiN_3$:Eu^{2+} Phosphors by the Self-Propagating High-Temperature Synthesis and Their Luminescent Properties. Chem Mater 19(18): 4592-4599.
12. Wang B, Lin H, Xu J, Chen H (2014) $CaMg_2Al_{16}O_{27}$:Mn^{4+}-based red phosphor: a potential color converter for high-powered warm W-LED. ACS Appl Mater Inter 6(24): 22905-22913.
13. Kim SJ, Jang HS, Unithrattil S, Kim YH (2016) Structural and luminescent properties of red-emitting $SrGe_4O_9$:Mn^{4+} phosphors for white light-emitting diodes with high color rendering index. J Lumin 172: 99-104.
14. Peng M, Yin X, Tanner PA, Liang C (2013) Orderly-Layered Tetravalent Manganese-Doped Strontium Aluminate $Sr_4Al_{14}O_{25}$:Mn^{4+}: An Efficient Red Phosphor for Warm White Light Emitting Diodes. J Am Ceram Soc 96(9): 2870-2876.
15. Lu W, Lv W, Zhao Q, Jiao M (2014) A novel efficient Mn^{4+} activated $Ca_{14}Al_{10}Zn_6O_{35}$ phosphor: application in red-emitting and white LEDs. Inorg Chem 53(22): 11985-11990.
16. Kim M, Park WB, Bang B, Kim CH (2015) Radiative and non-radiative decay rate of K_2SiF_6:Mn^{4+} phosphors. J Mater Chem C 3(21): 5484-5489.
17. Arai Y and Adachi S (2011) Optical properties of Mn^{4+}-activated Na_2SnF_6 and Cs_2SnF_6 red phosphors. J Lumin 131(12): 2652-2660.
18. Sekiguchi D, Nara J, Adachi S (2013) Photoluminescence and Raman scattering spectroscopies of $BaSiF_6$:Mn^{4+} red phosphor. J Appl Phys 113(18): 183-516.
19. Verstraete R, Sijbom HF, Joos JJ, Korthout K (2018) Red Mn^{4+}-Doped Fluoride Phosphors: Why Purity Matters. ACS Appl Mater Inter 10(22): 18845-18856.
20. Zhu YW, Shuo Y, Huang L, Liu Y (2019) Optimizing and adjusting the photoluminescence of Mn^{4+}-doped fluoride phosphors via forming composite particles. Dalton Trans 48(2): 711-717.
21. Fang MH, Yang TH, Lesniewski T, Lee C (2019) Hydrogen-Containing $Na_3HTi_{1-x}Mn_xF_8$ Narrow-Band Phosphor for Light-Emitting Diodes. ACS Energy Lett 4(2): 527-533.
22. Palumbo DT, Brown JJ (1970) Electronic States of Mn^{2+}-Activated Phosphors. J Electrochem Soc 117(9): 1184.
23. Kim JS, Kim JS, Kim TW, Kim SM (2005) Correlation between the crystalline environment and optical property of Mn^{2+} ions in $ZnGa_2O_4$:Mn^{2+} phosphor. Appl Phys Lett 86(9): 91912-91913.
24. Lei B, Li B, Wang X, Li W (2006) Green emitting long lasting phosphorescence (LLP) properties of Mg_2SnO_4:Mn^{2+} phosphor. J Lumin 118(2): 173-178.
25. Shang M, Li G, Yang D, Kang, X (2011) $(Zn,Mg)_2GeO_4$:Mn^{2+} submicrorods as promising green phosphors for field emission displays: hydrothermal synthesis and luminescence properties. Dalton Trans 40(37): 9379-9387.
26. Shi L, Huang Y, Seo HJ (2010) Emission red shift and unusual band narrowing of Mn^{2+} in $NaCaPO_4$ phosphor. J Phys Chem A 114(26): 6927-6934.
27. Polikarpov E, Catalini D, Padmaperuma A, Das P (2015) A high efficiency rare earth-free orange emitting phosphor. Opt Mater 46: 614-618.
28. Zhang ZJ, Delsing ACA, Notten PHL, Zhao JT (2013) Photoluminescence Properties of Red-Emitting Mn^{2+}-Activated $CaAlSiN_3$ Phosphor for White-LEDs. Ecs J Solid State Sc 2(4): R70-R75.
29. Lin YF, Chang YH, Chang YS, Tsai BS (2006) Photoluminescent properties of Ba_2ZnS_3: Mn phosphors. J Alloys Compd 421(1-2): 268-272.
30. Duan CJ, Otten WM, Delsing ACA, Hintzen HT (2008) Preparation and photoluminescence properties of Mn^{2+}-activated $M_2Si_5N_8$ (M=Ca, Sr, Ba) phosphors. J Solid State Chem 181(4): 751-757.
31. Collins BT (1993) Synthesis and Cathodoluminescence of Orange-Yellow- to Red-Emitting $Ca_{(1-x)}$ Mg_xS:Mn Phosphors. J Electrochem Soc 140(6): 1752.
32. Xie RJ, Hirosaki N, Li Y, Takeda T (2010) Rare-Earth Activated Nitride Phosphors: Synthesis, Luminescence and Applications. Mater 3(6): 3777-3793.
33. Liu L, Xie RJ, Hirosaki N, Takeda T (2009) Temperature Dependent Luminescence of Yellow-Emitting α-Sialon: Eu^{2+} Oxynitride Phosphors for White Light-Emitting Diodes. J Am Ceram Soc 92(11): 2668-2673.
34. Grün R (1979) The crystal structure of β-Si_3N_4: structural and stability considerations between α- and β-Si_3N_4. Acta Crystallographica Section B Structural Crystallography and Crystal Chemistry 35 (4): 800-804.
35. Xie RJ, Hirosaki N, Mitomo M, Yamamoto Y (2004) Optical properties of Eu^{2+} in α-SiAlON. J Phys Chem B 108(32): 12027-12031.
36. Jack KH (1976) Sialons and related nitrogen ceramics. J Mater Sci 11(6): 1135-1158.
37. Hampshire S, Park HK, Thompson DP, Jack KH (1978) α'-SiAlON ceramic. Nature 274(5674): 880-882.
38. Thorp HH (1992) Bond valence sum analysis of metal-ligand bond lengths in metalloenzymes and model complexes. Lnorg Chem 31(9): 1585-1588.
39. Liu W, Thorp HH (1993) Bond valence sum analysis of metal-ligand bond lengths in metalloenzymes and model complexes 2: Refined distances and other enzymes. lnorg Chem 32 (19): 4102-4105.
40. Palenik GJ (1997) Bond Valence Sums in Coordination Chemistry Using Oxidation State Independent R_0 Values A Simple Method for Calculating the Oxidation State of Manganese in Complexes Containing Only Mn−O Bonds. Lnorg Chem 36(21): 4888-4890.

41. Brown ID, Wu KK (1976) Empirical parameters for calculating cation–oxygen bond valences. Acta Crystallographica Section B Structural Crystallography and Crystal Chemistry 32(7): 1957-1959.

42. Ni J, Liu Q, Wan JQ, Liu GH (2018) Novel Luminescent Properties and Thermal Stability of Non-Rare-Earth Ca-α-sialon: Mn^{2+} Phosphors. J Lumin 202: 514-522.

43. Wang XJ, Xie RJ, Dierre B, Takeda T (2014) A novel and high brightness AlN: Mn^{2+} red phosphor for field emission displays. Dalton Trans 43(16): 6120-6127.

44. Duan CJ, Delsing ACA, Hintzen HT (2009) Photoluminescence Properties of Novel Red-Emitting Mn^{2+}-Activated MZnOS (M = Ca, Ba) Phosphors. Chem Mater 21(6): 1010-1016.

45. Shi Z, Zou Y, Jing R, Zhang K (2015) Red-emitting AlN: Mn^{2+} phosphors prepared by combustion synthesis. Func Mater Lett 8(2): 1550025.

46. Duan CJ, Delsing ACA, Hintzen HT (2009) Red emission from Mn^{2+} on a tetrahedral site in $MgSiN_2$. J Lumin 129(6): 645-649.

47. An JS, Noh JH, Cho IS, Roh HS (2010) Tailoring the Morphology and Structure of Nanosized Zn_2SiO_4:Mn^{2+} Phosphors Using the Hydrothermal Method and Their Luminescence Properties. J Phys Chem. C 114(23): 10330-10335.

48. Liu B, Wang Y, Wen Y, Zhang F (2012) Photoluminescence properties of S-doped $BaAl_{12}O_{19}$:Mn^{2+} phosphors for plasma display panels. Mater Lett 75: 137-139.

49. Izumi F, Mitomo M, Suzuki J (1982) Structure Refinement of Yttrium Alpha-Sialon from X-Ray-Powder Profile Data. J Mater Sci Lett 1(12): 533-535.

50. Blasse G, Bril A (1968) Fluorescence of Eu^{2+} activated alkaline-earth aluminates. Philips Res Rep 23(2): 201-206.

51. Blasse G, Wanamaker W (1968) Fluorescence of Eu^{+2} activated silicates. Philips Research Report 23: 189-189.

52. Dexter DL (1953) A Theory of Sensitized Luminescence in Solids. J Chem Phy 21(5): 836-850.

53. Chung CC, Jean JH (2010) Synthesis of Ca-α-SiAlON:Eux phosphor powder by carbothermal -reduction–nitridation process. Mater Chem Phys 123(1): 13-15.

54. Piao X, Machida K, Horikawa T, Hanzawa H (2008) Synthesis and luminescent properties of low oxygen contained Eu^{2+}-doped Ca-α-SiAlON phosphor from calcium cyanamide reduction. J Rare Earths 26(2): 198-202.

55. Cao CY, Yang HK, Chung JW, Moon BK (2011) Hydrothermal synthesis and enhanced photoluminescence of Tb^{3+} in Ce^{3+}/Tb^{3+} doped $KGdF_4$ nanocrystals. J Mater Chem 21(28): 10342-10347.

56. Yang W, Luo L, Chen TM, Wang NS (2005) Luminescence and Energy Transfer of Eu^{-} and Mn^{-}Coactivated $CaAl_2Si_2O_8$ as a Potential Phosphor for White-Light UVLED. Chem Mater 17(15): 3883-3888.

57. You H, Zhang J, Hong G, Zhang H (2007) Luminescent Properties of Mn^{2+} in Hexagonal Aluminates under Ultraviolet and Vacuum Ultraviolet Excitation. The Journal of Physical Chemistry C 111(28): 10657-10661.

DOI: 10.32474/MAMS.2020.02.000146